Title

Probing the bradycardic drug binding receptor of HCN-encoded pacemaker channels

Journal

Pflügers Archiv - European Journal of Physiology: European Journal of Physiology, 459(1)

ISSN

1432-2013

Authors

Chan, Yau-Chi
Wang, Kai
Wing Au, Ka
et al.

Publication Date

2009-11-01

DOI

10.1007/s00424-009-0719-2

Peer reviewed

Pflugers Arch - Eur J Physiol (2009) 459:25–38
DOI 10.1007/s00424-009-0719-2

CARDIOVASCULAR PHYSIOLOGY

Probing the bradycardic drug binding receptor of HCN-encoded pacemaker channels

Yau-Chi Chan · Kai Wang · Ka Wing Au · Chu-Pak Lau · Hung-Fat Tse · Ronald A. Li

Received: 3 February 2009 / Revised: 23 July 2009 / Accepted: 21 August 2009 / Published online: 8 September 2009

Abstract I_f (or I_h), encoded by the *h*yperpolarization-activated, *c*yclic *n*ucleotide-gated (HCN1–4) channel gene family, contributes significantly to cardiac pacing. Bradycardic agents such as ZD7288 that target HCN channels have been developed, but the molecular configuration of their receptor is poorly defined. Here, we probed the drug receptor by systematically introducing alanine scanning substitutions into the selectivity filter (C347A, I348A, G349A, Y350A, G351A in the P-loop), outer (P355A, V356A, S357A, M358A in the P-S6 linker), and inner (M377A, F378A, V379A in S6) pore vestibules of HCN1 channels. When heterologously expressed in human embryonic kidney 293 cells for patch-clamp recordings, I348A, G349A, Y350A, G351A, P355A, and V356A did not produce measurable currents. The half-blocking concentration (IC_{50}) of wild type (WT) for ZD7288 was 25.8±9.7 μM. While the IC_{50} of M358A was identical to WT, those of C347A, S357A, F378A, and V379A markedly increased to 137.6±56.4, 113.3±34.1, 587.1±167.5, and 1726.3±673.4 μM, respectively ($p<0.05$). Despite the proximity of the S6 residues studied, M377A was hypersensitive ($IC_{50}=5.1\pm0.7$ μM; $p<0.05$) implicating site specificity. To explore the energetic interactions among the S6 residues, double and triple substitutions (M377A/F378A, M377A/V379A, F378A/V379A, and M377A/F378A/V379A) were generated for thermodynamic cycle analysis. Specific interactions with coupling energies ($\Delta\Delta G$) >1 kT for M377–F378 and F378–V379 but not M377–V379 were identified. Based on these new data and others, we proposed a refined drug-blocking model that may lead to improved antiarrhythmics and bioartificial pacemaker designs.

Keywords Drug · Inner pore · ZD7288 · Pacemaker channels · HCN

Y.-C. Chan · K. Wang · K. Wing Au · C.-P. Lau · H.-F. Tse · R. A. Li
Division of Cardiology, Department of Medicine,
Queen Mary Hospital, Li Ka Shing Faculty of Medicine,
University of Hong Kong,
Pokfulam, Hong Kong

H.-F. Tse · R. A. Li
Stem Cell and Regenerative Medicine Program,
Research Center of Heart, Brain, Hormone, and Healthy Aging,
Li Ka Shing Faculty of Medicine, University of Hong Kong,
Pokfulam, Hong Kong

R. A. Li
Human Embryonic Stem Cell Consortium, School of Medicine,
University of California,
Davis, CA, USA

R. A. Li (✉)
Institute of Pediatric Regenerative Medicine, Shriners Hospital
for Children of North California, University of California,
Room 650, Shriners Hospital, 2425 Stockton Blvd.,
Sacramento, CA 95817, USA
e-mail: ronaldli@ucdavis.edu

Introduction

Pacemaker activity, the generation of spontaneous cellular electrical rhythms, governs numerous biological processes from the autonomous beating of the heart to respiratory rhythms and sleep cycles [31]. In the heart, abnormal pacing leads to various forms of arrhythmias (e.g., sick sinus syndrome). I_f (or I_h in noncardiac tissues), encoded by the *h*yperpolarization-activated, *c*yclic *n*ucleotide-gated (HCN1–4) channel gene family, is a key depolarizing current in cardiac pacing that is activated by hyperpolarization (rather than depolarization of classical voltage-gated

ion channels) [15, 23, 27]. Familial mutations of the human HCN genes have been described [24].

Structurally, each HCN channel consists of four homologous monomers pseudosymmetrically arranged around a central pore, resembling voltage-gated K^+ (K_v) channels; each of the four internal repeats is made up of six transmembrane segments (S1–S6; Fig. 1). The region between S5 and S6, or the so-called P-loop, inserts back into the membrane to form part of the pore. Indeed, the pore is analogous to the active site of an enzyme where major functional (e.g., ionic selectivity, conductance and gating) and pharmacological determinants are located [31].

Given the physiological importance of I_f, bradycardic drugs such as ZD7288 and ivabradine that target HCN channels have been developed. However, the molecular constituents of the HCN channel drug binding receptor have not been fully elucidated. A better understanding is crucial for designing more effective, HCN-specific drugs. For voltage-gated K^+ and Na^+ channels, their drug binding sites have been identified to reside in the pore regions [18]. Given the structural similarities between HCN and K_v channels, it has been hypothesized that the drug receptor of HCN channels is similarly located in the pore [5, 6, 12]. Shin and colleagues demonstrate that ZD7288 applied from the cytoplasmic side can enter and leave the inner pore of HCN1 channels only at voltages where the activation gate

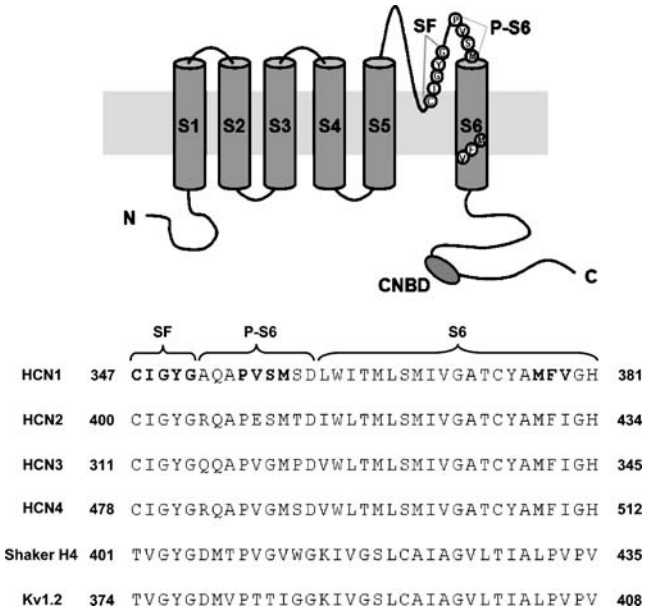

Fig. 1 Schematic diagram and sequence alignment of the HCN1 and K_V channels. *Upper panel*: the six putative transmembrane segments (*S1–S6*) of a monomeric HCN1 subunit. Ala scanning substitutions were introduced into three different regions: selectivity filter (*SF*; C347A, I348A, G349A, Y350A, G351A), outer (P355, V356, S357, M358), and inner (M377A, F378A, V379A) pore vestibule. *Lower panel*: the aligned amino acid sequences of HCN1-4 and K_v channels from the P-loop to S6. Substituted residues are highlighted in *bold*

Fig. 2 Effects of the Ala and Ile substitutions in the pore region on HCN1 currents. **a** *Upper panel*: representative recordings of WT HCN1 using the voltage protocol provided in the *inset*. *Trace a* −140 mV; *trace b* −100 mV; *trace c* −70 mV. Activation tail currents are enclosed in *dashed boxes* and magnified to the right. Steady-state activation relationship based on the tail current is also shown. *Lower panel*: representative traces of whole-cell currents recorded from cells expressing WT and different Ala-substituted constructs as indicated. **b** Immunostaining showed that the six dysfunctional constructs (I348A, G349A, Y350A, G351A, P355A, and V356A) were localized to the membrane surface, in a manner similar to that of WT

is opened [30]. Using site-directed mutagenesis, Sanguinetti and colleagues report that the S6 residues A425 and I432 of HCN2 channels (the analogous residues are A372 and V379 in HCN1) are primary determinants for ZD7288 block of wild-type (WT) HCN2 channels [12]. In the present study, we first identified additional novel HCN pore residues (C347, S357, M377, and F378 of HCN1) that are crucial for bradycardic drug binding then further explored their energetic interactions. Specific interactions with coupling energies ($\Delta\Delta G$) >1 kT for M377–F378 and F378–V379 but not M377–V379 were identified. These novel results are discussed in relation to the molecular composition of the HCN drug receptor and the mechanism of ZD7288 block as well as their implications in bradycardic drug and bioartificial pacemaker designs.

Materials and methods

Molecular biology and heterologous expression Murine HCN1 cDNA was cloned from mouse brain RNA [27] and subcloned into the mammalian expression vector pCI (Promega, Madison, WI, USA). Desired substitutions were constructed as previously described [38]. HCN1 channels were transiently expressed in human embryonic kidney 293 cells (HEK293) using Lipofectamine Plus 2000 (Invitrogen, Carlsbad, CA, USA). For identifying HCN1-expressing cells, the channel plasmid was cotransfected with pCI-green fluorescent protein (GFP) with a ratio of 10:1. Twenty-four hours to 48 h after transfection, cells were trypsinized and plated on glass-bottomed culture dishes 2 h prior to patch-clamp or immunohistochemical experiments.

Electrophysiology Whole-cell patch-clamp recordings were performed using an EPC-10 patch-clamp amplifier (HEKA electronic, Heidelberg, Germany). Only GFP-expressing HEK293 cells as identified by their epifluorescence with an excitation wavelength of 488 nm were selected for experiments. All recordings were performed at room temperature in a bath solution containing (in mM): 110 NaCl, 30 KCl, 1.8 $CaCl_2$, 0.5 $MgCl_2$, 5 HEPES, and 10 glucose, pH adjusted to 7.4 with NaOH. The internal solution contained (in mM): 10 NaCl, 130 KCl, 0.5 $MgCl_2$, 5 HEPES, 1

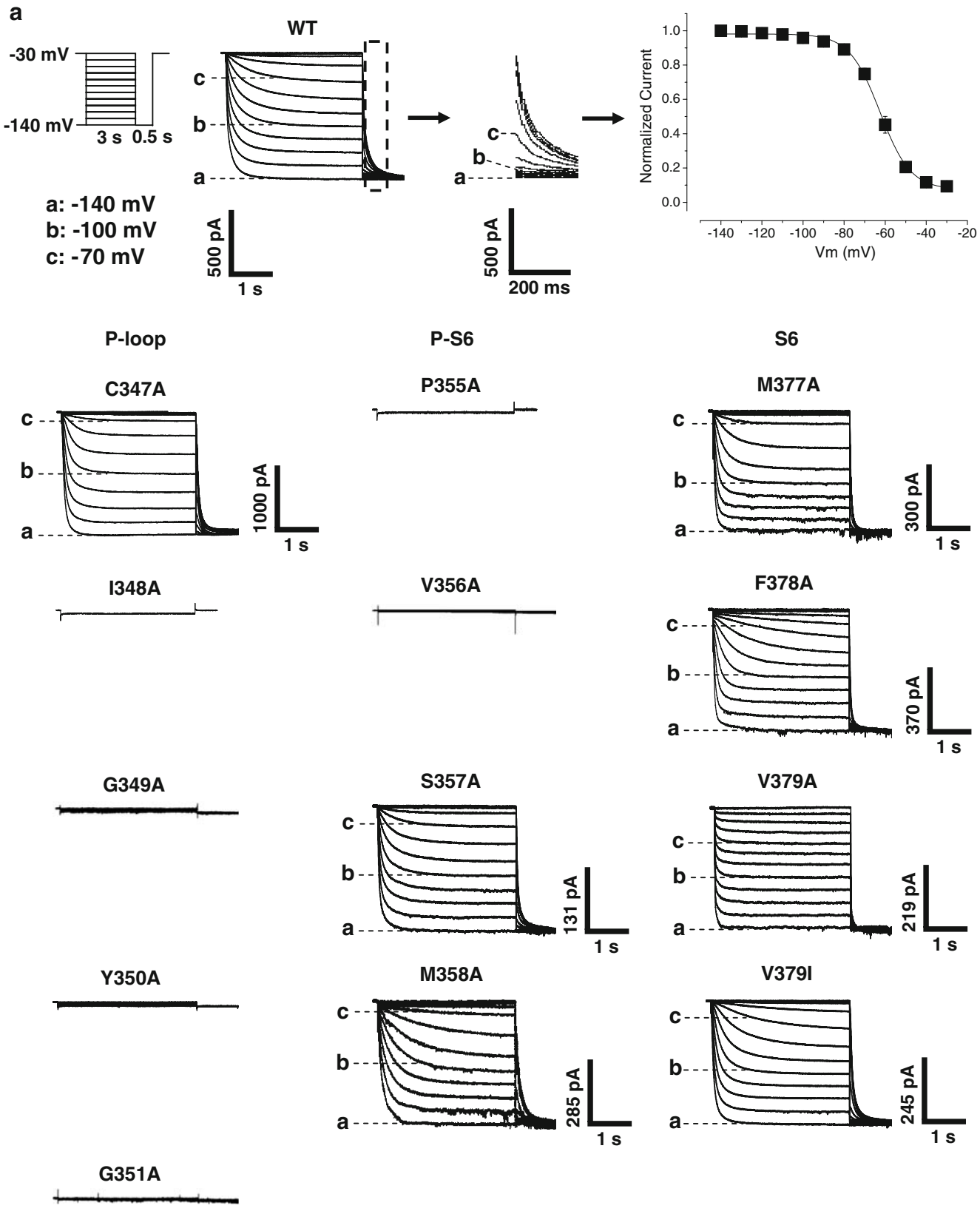
a
WT
-30 mV
-140 mV
3 s 0.5 s
c
b
a
a: -140 mV
b: -100 mV
c: -70 mV
500 pA
1 s
500 pA
200 ms
Normalized Current
Vm (mV)
P-loop
P-S6
S6
C347A
P355A
M377A
1000 pA
300 pA
I348A
V356A
F378A
370 pA
G349A
S357A
V379A
131 pA
219 pA
Y350A
M358A
V379I
285 pA
245 pA
G351A
1 s

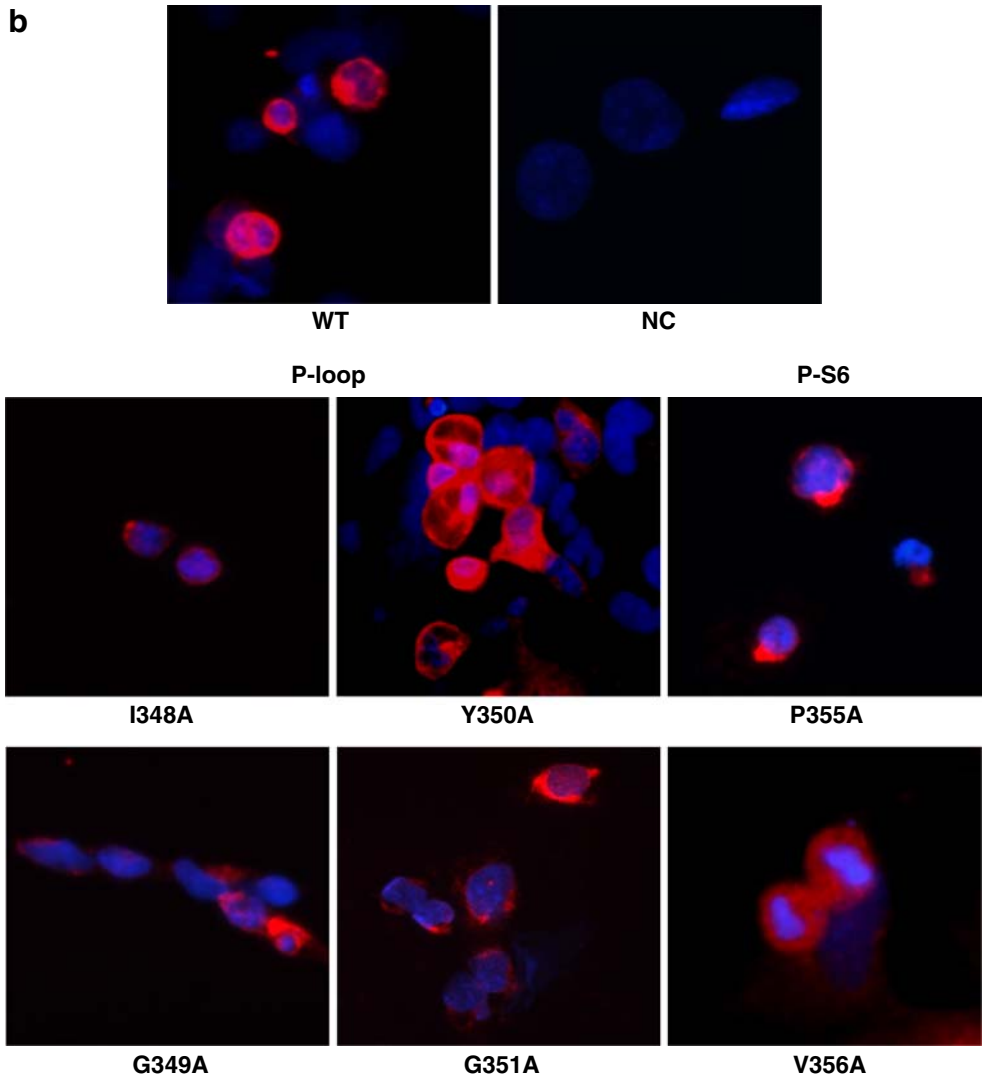

Fig. 2 (continued)

EGTA, and 5 MgATP, pH adjusted to 7.3 with KOH. The electrode tip and series resistances were, respectively, ~3–4 and <10 MΩ. The sampling frequency was 1.25 kHz. Cell capacitance and series resistance compensation were not used. The cycle length of the protocols was 4.6 s. The potentials were not corrected for the liquid junction potentials of +20.3 mV.

Experimental protocols and data analysis The steady-state current–voltage (*I–V*) relationship was determined by plotting currents measured at the end of a 3-s pulse ranging from −140 to −30 mV from a holding potential of −30 mV against the test potentials. The voltage dependence of HCN channel activation was assessed by plotting tail currents measured immediately after pulsing to −140 mV as a function of the preceding 3-s test pulse normalized to the maximum tail current recorded. The data were fitted to the Boltzmann functions using the Marquardt–Levenberg algorithm in a nonlinear least squares procedure:

$$m = 1/\left(1 + \exp\left(\left(V_t - V_{\frac{1}{2}}\right)/k\right)\right)$$

where V_t is the test potential; $V_{1/2}$ is the half-point of the relationship; $k=RT/zF$ is the slope factor, and R, T, z, and F have their usual meanings.

For half-blocking concentrations (IC_{50}), the following binding isotherm was used:

$$I/I_O = 1/(1 + ([\text{blocker}]/IC_{50})^n)$$

Fig. 3 Steady-state current voltage and activation curves. **a** Effects of Ala and Ile substitutions on HCN1 steady-state current–voltage relationships. **b** Representative tracings and steady-state activation relationships

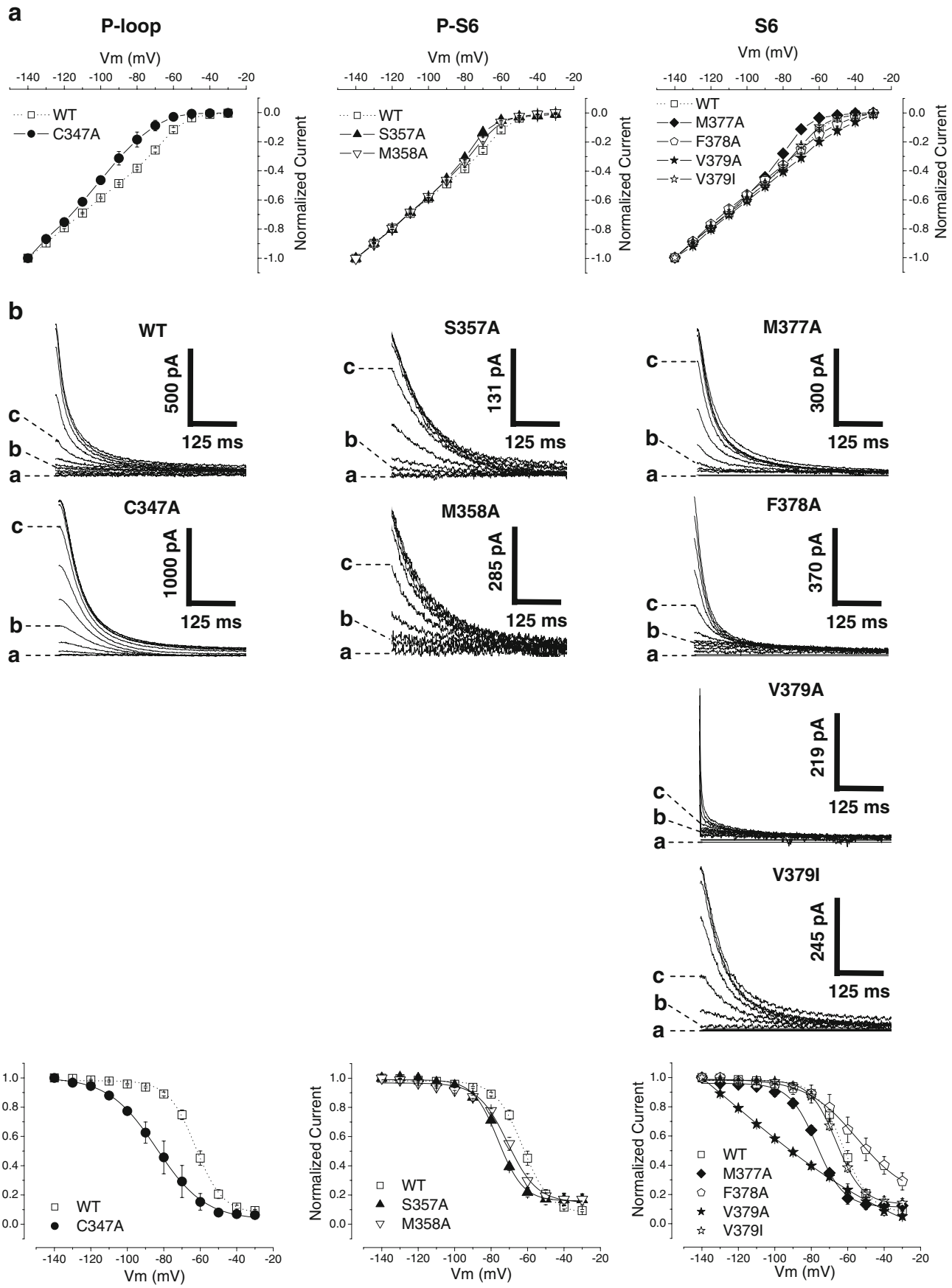
a
P-loop
P-S6
S6
Vm (mV)
-140 -120 -100 -80 -60 -40 -20
WT
C347A
S357A
M358A
M377A
F378A
V379A
V379I
Normalized Current
0.0 -0.2 -0.4 -0.6 -0.8 -1.0
b
WT
500 pA
125 ms
S357A
131 pA
M377A
300 pA
C347A
1000 pA
M358A
285 pA
F378A
370 pA
V379A
219 pA
V379I
245 pA
c
b
a
Normalized Current
1.0 0.8 0.6 0.4 0.2 0.0
Vm (mV)

where n is the Hill coefficient; I_O and I are the peak currents measured at the voltage indicated before and after blocker application, respectively. All IC_{50} values reported were calculated from individual determinations.

For thermodynamic cycle analysis [17], coupling coefficients (Ω) and interaction energies ($\Delta\Delta G$) for various mutant channel pairs were calculated from the corresponding IC_{50} values with the equations below:

$$\Omega = \left(IC_{50}^{ConstructA}/IC_{50}^{ConstructAB}\right)/\left(IC_{50}^{WT}/IC_{50}^{ConstructB}\right)$$
$$\Delta\Delta G = RT\ 1n\ \Omega$$

where R is the gas constant ($k \times N_A$), and T is the absolute temperature. The standard errors for $\Delta\Delta G$ were estimated by dividing the square root of the sum of the variances of the RT ln IC_{50} means by the square root of the degree of freedom. Significant interactions were defined as $\Delta\Delta G >$ 1 kcal/mol as we and others previously reported [20]. All data presented were the means±SEM. Statistical significance ($p<0.05$) was determined using an unpaired Student's t test.

Immunostaining HEK293 cells were fixed in 4% paraformaldehyde for 15 min at 21°C, washed with phosphate-buffered saline (PBS), and permeabilized with 0.1% Trition-X-100/PBS. The cells were then blocked with 10% bovine serum albumin with 4% goat serum in PBS for 2 h at 21°C. Fixed cells were incubated with the HCN1 rabbit polyclonal antibodies (Alomone Labs, Jerusalem, Israel) at a dilution of 1:200 overnight at 4°C, followed by incubation with fluorescent-labeled secondary antibodies for 50 min at 21°C and visualization by fluorescent microscopy.

Results

Effects of alanine (Ala) substitutions on HCN1 As a first step, we generated a total of 12 singly Ala-substituted HCN1 pore constructs that correspond to these regions: C347A, I348A, G349A, Y350A, and G351A in the ascending limb of the P-loop, P355A, V356A, S357A, and M358A in the P-S6 linker that forms part of the extrapore and M377A, F378A, and V379A in the S6 segment that constitutes part of the cytoplasmic pore mouth (Fig. 2a). Of note, I432 of HCN2, the analogous residue to V379 of HCN1, has been previously reported to involve in ZD7288 interaction [12]. Taken together with the notion that aromatic residues in S6 of K and Na channels participate in drug binding, we therefore hypothesized that the $MFV_{377–379}$ triplet also contributes to ZD7288 binding. As anticipated from our previous results [38], substituting residues 349–351 of the GYG motif (i.e., G349A, Y350A, G351A) that is crucial for permeation did not produce measurable currents. I348A, P355A, and V356A channels were also not functional. Immunostaining indicated that all nonfunctional constructs were membrane-localized similar to WT (Fig. 2b), suggesting that the loss of function did not result from defects in protein synthesis or trafficking. In stark contrast, all of C347A, S357A, M358A, M377A, F378A, and V379A channels expressed robust time-dependent hyperpolarization-activated currents (Fig. 2a). The corresponding steady-state current–voltage (I–V) relationships are shown in Fig. 3a. The different activation thresholds hint that the gating properties of some of these Ala-substituted pore constructs have been altered. To test this notion, we next examined their steady-state activation properties (Fig. 3b). Indeed, all of C347A (P-loop), S357A, and M358A (P-S6), M377A, and V379A (S6) similarly and significantly hyperpolarized the steady-state activation midpoint ($V_{1/2,\ Con}$) of WT from −62.6±1.4 mV (n=6) to −82.1±4.7 (n=3), −76.1±0.3 (n=3), −70.8±1.6 (n=5), −77.4±1.6 (n=4) and −97.8±2.6 (n=8) mV, respectively ($p<0.05$). By contrast, F378A (of S6) caused a noticeable opposite depolarizing shift ($V_{1/2,\ Con}$=−56.2±3.7 mV, n=3) although the difference did not reach statistical significance (p=0.09). Of note, C347A, F378A, and V379A increased the slope factor (k) by ~2-fold, twofold, and fivefold, respectively ($p<0.05$).

Effects of Ala substitutions on current blockade by ZD7288 To investigate the effect of our pore substitutions on drug block, we started by characterizing the response of WT HCN1 to ZD7288. Figure 4a shows that ZD7288 dose-dependently reduced the maximum steady-state current of WT at −140 mV. The half-blocking concentration or IC_{50} estimated from the binding curve was 25.8±9.7 μM (n=5). The steady-state I–V and activation curves recorded in the absence and presence of ZD7288 are given in Fig. 4b, c, respectively. Figure 5 summarizes the effect of Ala substitutions on ZD7288 blockade. C347A, S357A, F378A, and V379A significantly shifted the binding curve in the rightward direction. Their IC_{50}s were 137.6±56.4 (n=4), 113.3±34.1 (n=5), 587.1±167.5 (n=3), and 1,726.3± 673.4 μM (n=3), respectively. Despite the proximity of M377 to F378 and V379 in the primary sequence of S6, its Ala substitution exerted an opposite effect on ZD7288 block

Fig. 4 ZD7288 block of mHCN1 channels. **a** Representative current tracings and dose–response relationship for ZD7288 block of WT HCN1 channel. Normalized steady-state currents at −140 mV were plotted as a function of extracellular ZD7288 concentrations. Data points were fitted with a binding isotherm to estimate the IC_{50} for ZD7288 of the channel. **b** The steady-state current–voltage relationships of WT HCN1 channel in the absence and presence of ZD7288. **c** The corresponding steady-state activation curves for WT HCN1 channel. **d** The steady-state activation curves for the mutant HCN1 channels

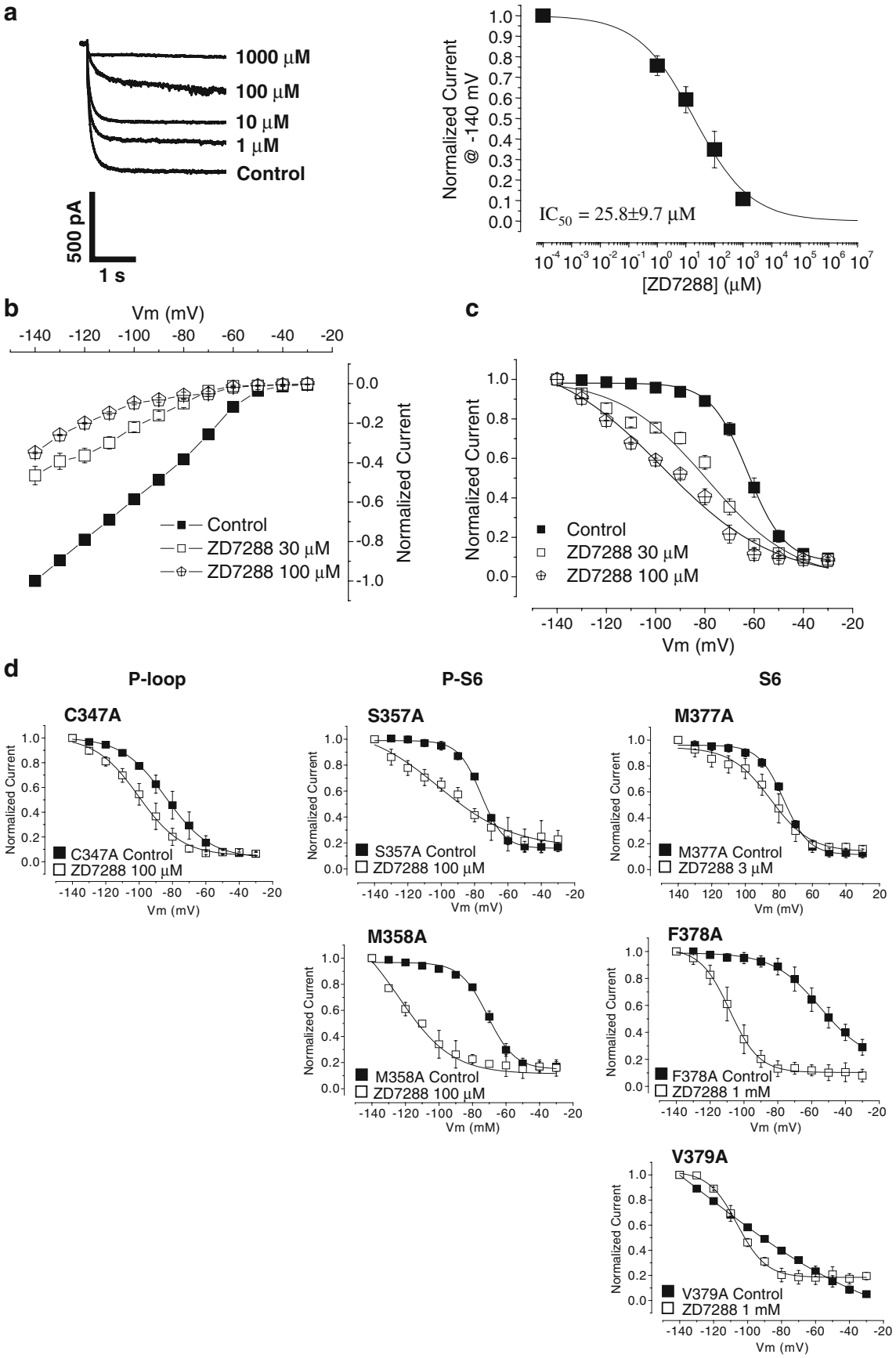
a
1000 μM
100 μM
10 μM
1 μM
Control
500 pA
1 s
Normalized Current @ -140 mV
IC50 = 25.8±9.7 μM
[ZD7288] (μM)
b
Vm (mV)
Control
ZD7288 30 μM
ZD7288 100 μM
Normalized Current
c
Normalized Current
Control
ZD7288 30 μM
ZD7288 100 μM
Vm (mV)
d
P-loop
P-S6
S6
C347A
C347A Control
ZD7288 100 μM
S357A
S357A Control
ZD7288 100 μM
M377A
M377A Control
ZD7288 3 μM
M358A
M358A Control
ZD7288 100 μM
Vm (mM)
F378A
F378A Control
ZD7288 1 mM
V379A
V379A Control
ZD7288 1 mM
Normalized Current
Vm (mV)

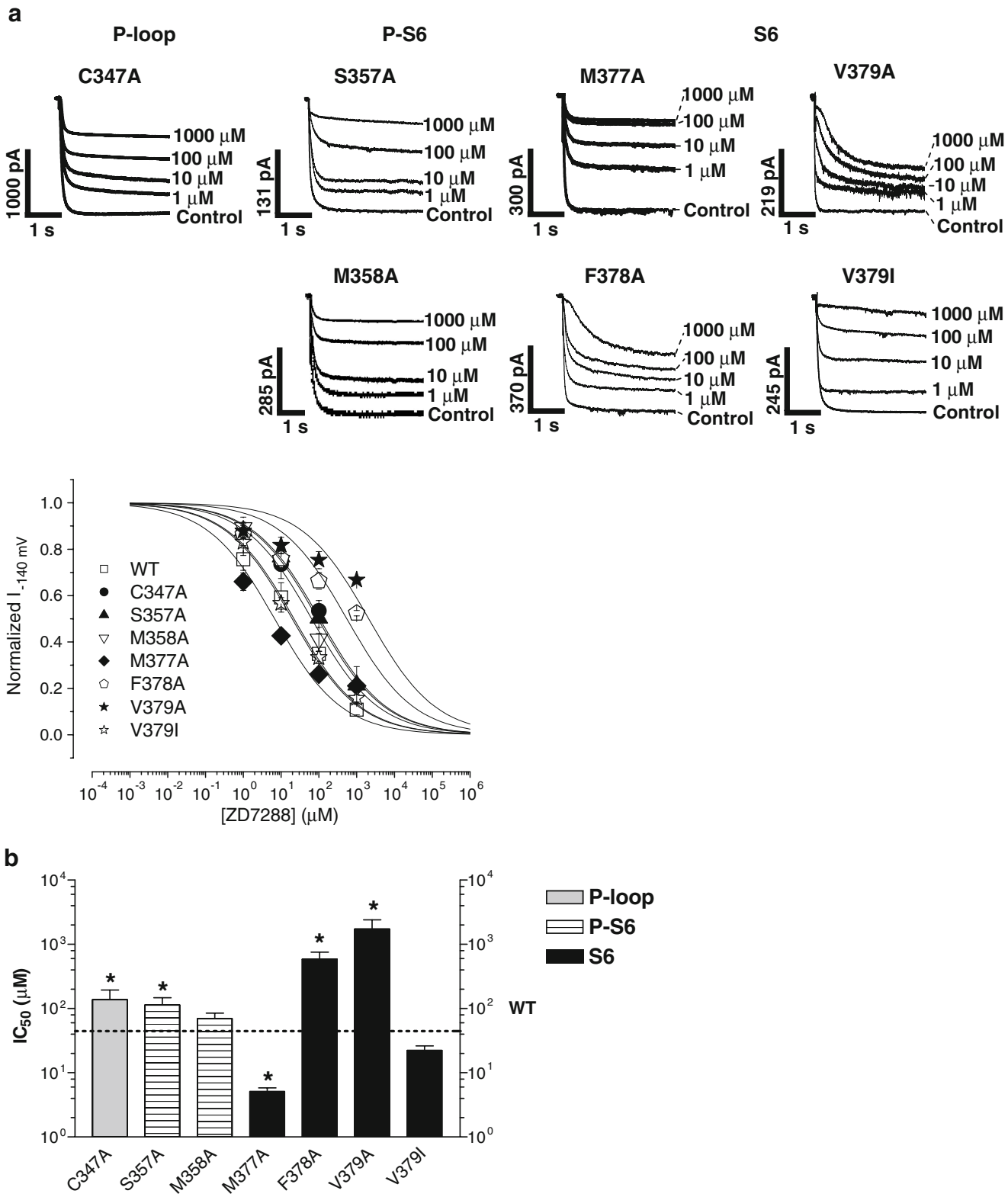

Fig. 5 Effects of Ala substitutions on ZD7288 block. **a** *Upper panel*: current tracings recorded at −140 mV in the presence of ZD7288 at different concentrations. *Lower panel*: the dose–response curves. **b** Summary of IC_{50}. *Dashed line* indicates the level of WT sensitivity (*, $p<0.05$)

(IC_{50}=5.1±0.7 μM, n=3; p<0.05). The Met-to-Ala at residue 358 (i.e., M358A), however, was not different from WT (p>0.05). Collectively, these observations suggest that the effects of our Ala pore substitutions on ZD7288 block were site specific. Similar to the hyperpolarizing shifts observed for WT HCN1 channels, ZD7288 likewise caused leftward activation shifts curves of Ala-substituted HCN channels at concentrations comparable to the corresponding IC_{50}s. Interestingly, 1 mM ZD7288 nearly restored the WT slope factor of V379A. These results hint at a gating effect of ZD7288 on HCN channels as do local anesthetics on K^+ and Na^+ channel gating.

Energetic interactions among the $MFV_{377–379}$ triplet in S6 Among all the pore sites investigated, the S6 residues of the $MFV_{377–379}$ triplet, which are in close proximity to each other, when Ala-substituted produced the most significant changes in their responses to ZD7288 and gating properties, consistent with the role of S6 residues in drug binding. To explore their energetic interactions, three double (M377A/F378A, M377A/V379A, and F378A/V379A) and triple substitutions (M377A/F378A/V379A) were generated for thermodynamic cycle analysis. All constructs led to robust current expression. As for ZD7288 blockade assessed at −140 mV, the IC_{50} values as estimated from the dose–response curves of M377A/F378A, M377A/V379A, F378A/V379A, and M377A/F378A/V379A channels were 2,253.8±378.6 (n=6), 313.5±79.4 (n=4), 1,267.0±484.1 (n=6), and 2,027.4±1,100.9 μM (n=4), respectively (Fig. 6; p<0.05). To calculate their interaction energies with each other, a representative cycle analysis was given in Fig. 7a as illustration. The coupling coefficient (Ω) for the interaction pair M377–F378 calculated from WT, M377A, F378A, and M377A/F378A was 0.05±0.01. Using the corresponding single and double substitutions, the M377–V379 and F378–V379 pairs were calculated to have Ωs of 1.09±0.21 and 31.0±9.09, respectively. Their absolute interacting energies were −1.77±0.09, 0.05±0.13, and 2.03±0.18 kcal/mol, respectively (Fig. 7b). These results indicate that significant interactions exist for the pairs M377–F378 and F378–V379 but not M377–V379.

As a means to verify the specificity of our results presented above, we constructed the triple construct M377A/F378A/V379A for further cycle analyses. To calculate the interaction of the pair M377–F378 in the background of V379A, the combination of V379A, M377A/V379A, F378A/V379A, and M377A/F378A/V379A was employed. The Ω and $\Delta\Delta G$ calculated for the pair were 0.11±0.01 and −1.31±0.10 kcal/mol (or −2.21±0.15 kcal/mol), respectively. Using the same approach, the Ω and $\Delta\Delta G$ for the pairs of F378–V379 in the M377A background and M377–V379 in the F378A background were 68.17±9.09 and 4.22±0.54 and 2.40±0.21 and 0.88±0.24 kcal/mol, respectively. In other words, the same rank order for interactions as those calculated from WT and single and double substitutions was observed.

V379I displayed WT gating and ZD7288 phenotypes Isoform-specific differences in bradycardic drug block of HCN1 and HCN4 by the ivabradine have been reported [7]. Of note, the analogous residues of V379 of HCN1 are isoleucines in HCN2, HCN3, and HCN4 (Fig. 1). However, V379I displayed gating and ZD7288 sensitivity not different from WT (Figs. 2, 3, and 5).

Discussion

In the present study, we probed the molecular constituents of the drug binding receptor in HCN channels by Ala scanning mutagenesis of three distinct pore regions: the selectivity filter and the outer and the inner pore vestibules. Among the pore residues examined, the S6 triplet $MFV_{377–379}$ appears to play the most significant role in determining the WT drug-blocking phenotype. When Ala-substituted, residues M377, F378, and V379 significantly affected the sensitivity of HCN1 channels to the bradycardic drug ZD7288 by up to 67-fold (versus the ~3-fold differences of the P- and P-S6 constructs). This finding is consistent with the notion that the inner pore region is crucial for drug binding as demonstrated by numerous previous K_v and Na_v channel studies [18]. Despite their proximity in the primary sequence, M377A enhanced whereas F378A and V379A reduced ZD7288 block. Furthermore, thermodynamic cycle analysis revealed that the pairs M377–F378 and F378–V379, but not M377–V379, energetically interact. Importantly, whereas M377 and F378 negatively interact with other in drug binding, the interaction between residues F378 and V379 is positive. The same common pattern was observed when channel backgrounds other than WT were employed for cycle analyses. These differential effects strongly support that the observed changes in ZD7288 block were highly site specific.

Sequence alignments and comparison with the known crystal structures of K_v channels suggest that the side chain of S6-V379 of HCN1 faces the aqueous phase of the cytoplasmic pore. In *Shaker* K^+ channels, the hydrophobic binding pocket for quaternary ammonium compounds consists of T469 in S6 [13]; the analogous residue of *Shaker*'s T469 in HCN1 is C374. Our results indicate that C347A display a fourfold reduction in ZD7288 sensitivity. Taken together with the present findings that the S6 substitutions F378A and V379A (but not M377A) reduce ZD7288 block, we propose that residues F378 and V379 are located on the same side of the S6-$MFV_{377–379}$ helical

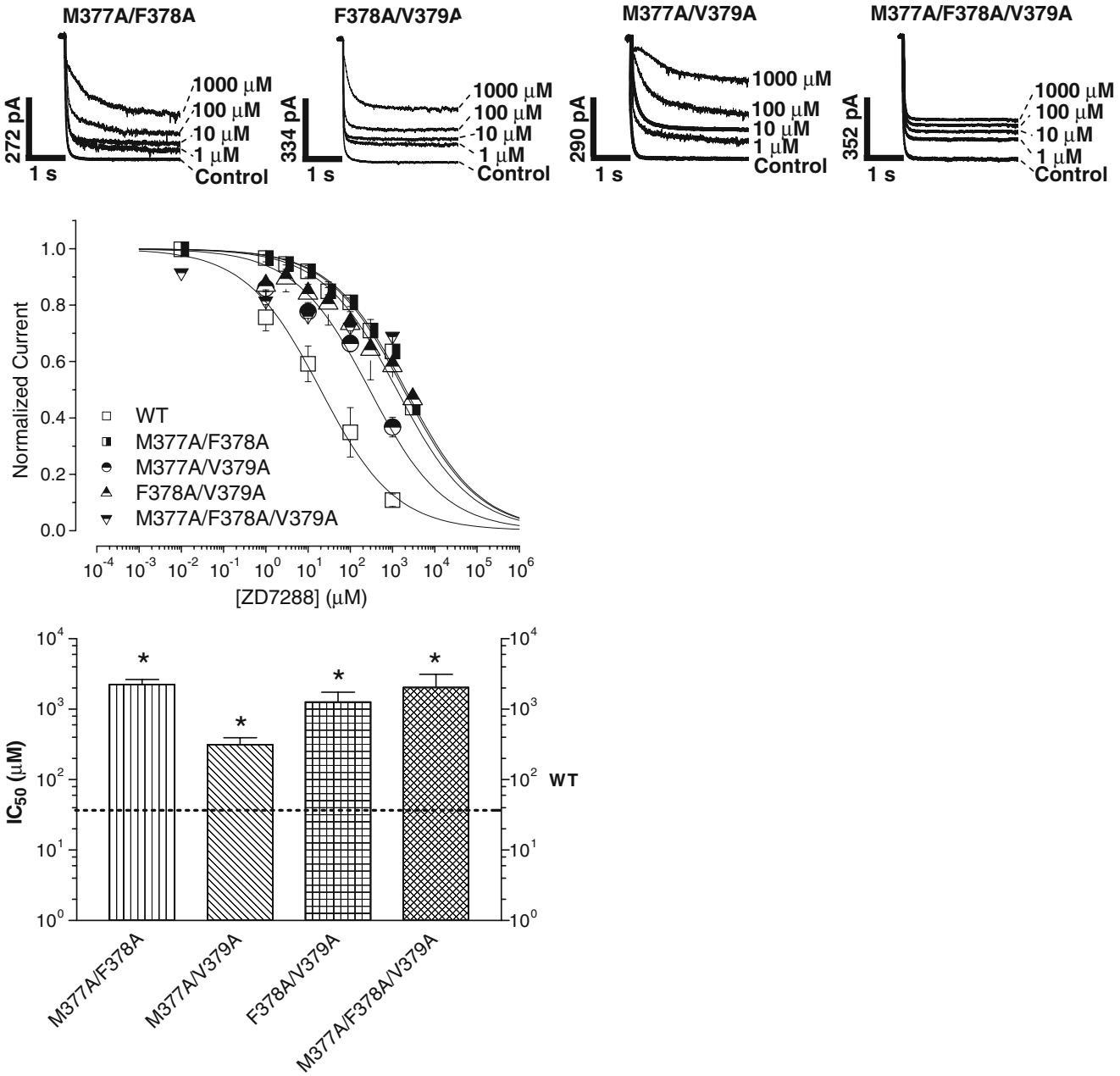

Fig. 6 Effects of double and triple Ala substitutions on ZD7288 block. *Upper panel*: the current tracings recorded at −140 mV in the presence of ZD7288 at different concentrations. *Middle panel*: the dose–response curves for ZD7288 block of the WT, double and triple HCN1 channels. *Lower panel*: bar graph summarizing the IC_{50}. *Dashed line* indicates the level of WT sensitivity. *Asterisks* indicate statistical differences (*$p<0.05$) compared with WT

turn that is exposed to the cytoplasmic pore. This spatial arrangement is consistent with our thermodynamic cycle analysis that energetic interactions exist only for the pairs M377–F378 and F378–V379 but not M377–V379. Along with the P-loop residue C374, the F378/V379 helical face forms a receptor pocket to which ZD7288 binds. Although the S6 residue M377 faces a different side of the S6-$MFV_{377–379}$ helix, it regulates the pathway by which the drug molecule travels to its F378–V379 binding pocket: when M377 is substituted by the smaller alanine, drug access is improved, sterically and/or by relieving some negative interactions, thereby facilitating ZD7288 block. This proposed mechanism is also consistent with the negative coupling identified for the M377–F378 pair. Our model is schematically presented in Fig. 8.

Although chemical and structural differences exist for ZD7288 and other HCN channel blockers (such as ivabradine, cilobradine, and zatebradine), Ile432 of

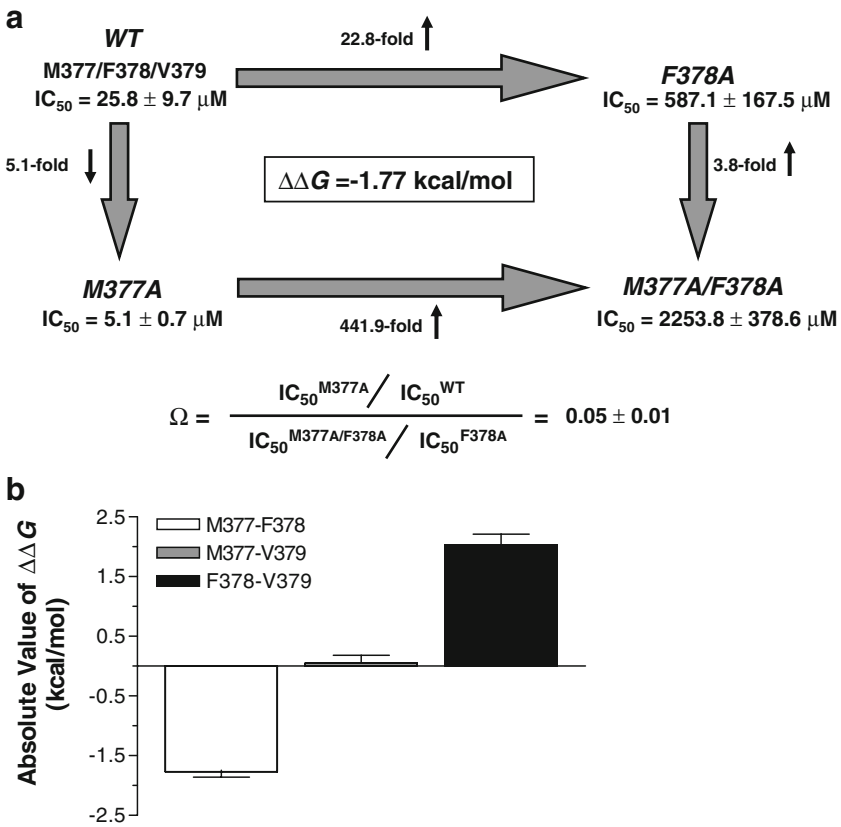

Fig. 7 Interaction energies of the pairs M377–F378, F378–V379, and M377–V379. **a** A representative cycle analysis of the interaction pair M377–F378. **b** *Bar graph* showing the absolute interaction energies ($\Delta\Delta G$) for the pairs M377–F378, M377–V379, and F378–V379

HCN2, a residue homologous to Val379 in the $MFV_{377–379}$ triplet of HCN1, has also been shown to be involved in cilobradine binding [12]. Further investigations will be needed to test whether there is a single common receptor in HCN channels for these drugs or there are multiple overlapping and/or nonoverlapping drug binding sites. The interacting MFV triplet that we have identified in the present study appears to be a prime candidate for testing these possibilities.

Though we have identified key residues that determine ZD7288 block of HCN1 channels and energetically quantified their interactions, the nature of their side chain interactions with ZD7288 remains to be explored. The spatial proximity of these key residues during the drug-bound state, their accessibility, state dependent or not, from the extracellular and cytoplasmic sides also require additional experiments (e.g., cysteine scanning mutagenesis). For nonfunctional single Ala-substituted channels, the generation of tandem constructs with one, two, or three copies of a mutation introduced the pore may shed insights into their roles in drug block.

To date, four isoforms, namely HCN1–4, have been identified. These isoforms exhibit different patterns of gene expression and tissue distribution [23, 25–28] and coassemble to form heteromeric complexes (except between HCN2 and HCN3) that underlie the native I_f [11, 36, 38]. Although the primary sequences of the HCN1-4 pores are highly conserved, three of the residues substituted in this study, V356, S357, and V379, are isoform variants (Fig. 1). While S357A only modestly contributes to ZD7288 binding and V356A abolishes channel function (which prevents any direct conclusion about its pharmacological role to be drawn), we have identified V379 as a determinant of drug sensitivity and proposed that it constitutes part of the drug receptor. The isoforms HCN1 and HCN2 are known to display different drug sensitivities. Although residue 379 is an isoform variant, V379I has gating properties and ZD7288 sensitivity not different from WT murine HCN1. Thus, further experiments will be needed to investigate the basis of isoform-specific drug block. In stark contrast, the homologous substitution V390I in human HCN1 markedly increases the ZD7288 sensitivity rendering it HCN2-like [12]. These results suggest that species- as well as isoform-specific differences in drug block exist. Further experiments will be needed to investigate the basis of these differences. Given the fact that native I_f (or I_h) currents from various tissues have diverse molecular identities due to the different isoforms expressed and their coassembly, a better understanding of drug block of HCN1–4 channels is crucial for developing tissue-selective I_f blockers.

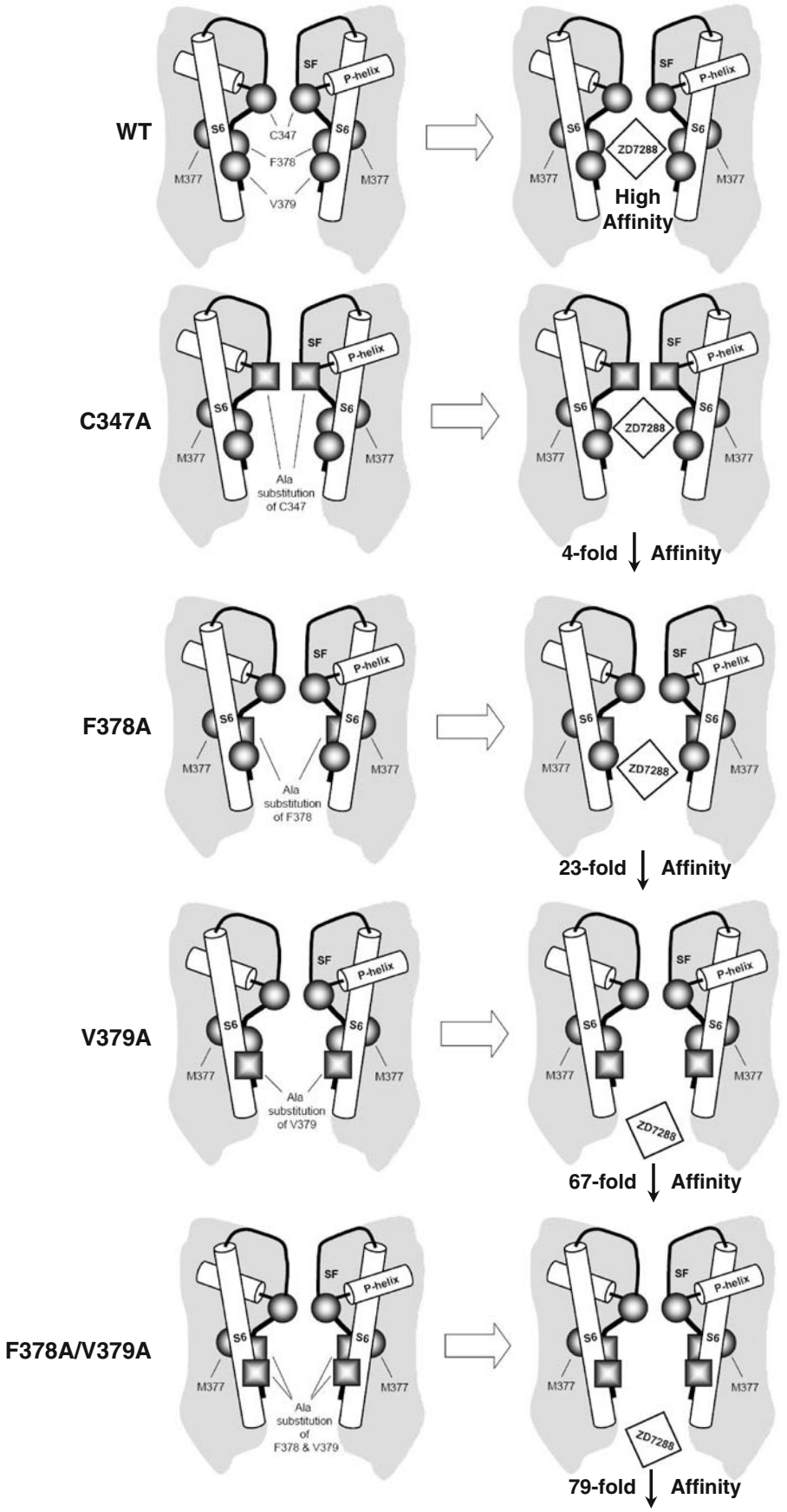

Fig. 8 Schematic diagram showing the proposed model of ZD7288 binding to its receptor constituted by C347, F378, and V379. See text for details

HCN-encoded I_f (or I_h) is one of the key players that prominently modulate the rhythmic firing activity of cardiac nodal pacemaker. For the heart, idiopathic and familial sinus dysfunctions associated with human HCN mutations have been reported [24, 29]. Although cardiac I_f is most abundant in the sino-atrial node, it is also found at various levels in the atrioventricular node, the Purkinje fibers, the atria, and the ventricles [8, 9, 14]. Indeed, upregulation of I_f has been suggested to contribute to atrial ectopy and other arrhythmias associated with heart failure, hypertrophy, and hypertension [8, 9, 14]. As a result, drugs that target HCN channels such as ivabradine, ZD7288, have been developed. Using an engineered HCN1 channel with the S3–S4 linker residues 277–279 deleted [33, 34], we have successfully constructed an *in vivo* bioartificial cardiac pacemaker that suffices to replace or supplement conventional electronic devices in a large animal sick sinus syndrome model [35, 39]. Thus, our present results may be useful for designing future HCN drugs and engineered HCN channels with a custom-tailored modulatory drug receptor for gene- [35, 39] and cell-based [21, 32] therapies. For instance, the substitution M377A can be combined with others to generate a bioartificial pacemaker that is ultrasensitive to bradycardiac drugs to confer drug specificity and to minimize potential side effects (due to blockade of endogenous I_f or I_h in other tissues).

Of note, the HCN1 isoform examined in the present study is the least sensitive to cAMP among HCN1–4. HCN1 has been chosen because we have previously extensively studied its structure–function properties [1–4, 16, 19, 31, 33, 34, 37, 38]. Indeed, we have even successfully employed an engineered HCN1 channel for constructing bioartificial pacemakers both in vitro and in vivo [10, 22, 35, 39]. Although the least sensitive, HCN1 nonetheless responds to adrenergic stimulations [35]. The present results will also be particularly useful for improving antiarrhythmic designs and selectivity. Nevertheless, further experiments at physiological temperature, though more technically difficult to perform and thus missed in the present study [40], will be useful to examine the temperature-dependent effect as low temperatures was shown to possibly attenuate I_f inhibition [41].

In summary, we conclude that pore residues C347, F378, and V379 of HCN1 channels are crucial for ZD7288 block. Together, these amino acids may constitute part of the drug binding receptor that is located relatively deep into the pore. These P-loop and the S6 residues exert their effects by modulating drug access to the receptor and by stabilizing the drug-bound HCN channel complex. Therefore, we proposed a refined drug-blocking model that may lead to more improved antiarrhythmics and bioartificial pacemaker designs, in particular, to provide better insights in improving drug selectivity.

Grants This work was supported by grants from the NIH (R01 HL72857 to RAL), the Stem Cell Program of the University of California, Davis School of Medicine (to RAL), the Hong Kong Research Grant Council (7459/04M to CPL, HFT, and RAL), and the CC Wong Stem Cell Fund (to HFT and RAL).

References

1. Au KW, Siu CW, Lau CP, Tse HF, Li RA (2008) Structural and functional determinants in the S5-P region of HCN-encoded pacemaker channels revealed by cysteine-scanning substitutions. Am J Physiol 294:C136–144
2. Azene EM, Sang D, Tsang SY, Li RA (2005) Pore-to-gate coupling of HCN channels revealed by a pore variant that contributes to gating but not permeation. Biochem Biophys Res Commun 327:1131–1142
3. Azene EM, Xue T, Li RA (2003) Molecular basis of the effect of potassium on heterologously expressed pacemaker (HCN) channels. J Physiol 547:349–356
4. Azene EM, Xue T, Marban E, Tomaselli GF, Li RA (2005) Non-equilibrium behavior of HCN channels: insights into the role of HCN channels in native and engineered pacemakers. Cardiovasc Res 67:263–273
5. Baruscotti M, Bucchi A, Difrancesco D (2005) Physiology and pharmacology of the cardiac pacemaker ("funny") current. Pharmacol Ther 107:59–79
6. Bucchi A, Baruscotti M, DiFrancesco D (2002) Current-dependent block of rabbit sino-atrial node I(f) channels by ivabradine. J Gen Physiol 120:1–13
7. Bucchi A, Tognati A, Milanesi R, Baruscotti M, DiFrancesco D (2006) Properties of ivabradine-induced block of HCN1 and HCN4 pacemaker channels. J Physiol 572:335–346
8. Cerbai E, Barbieri M, Mugelli A (1994) Characterization of the hyperpolarization-activated current, I(f), in ventricular myocytes isolated from hypertensive rats. J Physiol 481(Pt 3):585–591
9. Cerbai E, Sartiani L, DePaoli P, Pino R, Maccherini M, Bizzarri F, DiCiolla F, Davoli G, Sani G, Mugelli A (2001) The properties of the pacemaker current I(F)in human ventricular myocytes are modulated by cardiac disease. J Mol Cell Cardiol 33:441–448
10. Chan YC, Siu CW, Lau YM, Lau CP, Li RA, Tse HF (2009) Synergistic effects of inward rectifier (I_{K1}) and pacemaker (I_f) currents on the induction of bioengineered cardiac automaticity. J Cardiovasc Electrophysiol 20:1048–1054
11. Chen S, Wang J, Siegelbaum SA (2001) Properties of hyperpolarization-activated pacemaker current defined by coassembly of HCN1 and HCN2 subunits and basal modulation by cyclic nucleotide. J Gen Physiol 117:491–504
12. Cheng L, Kinard K, Rajamani R, Sanguinetti MC (2007) Molecular mapping of the binding site for a blocker of hyperpolarization-activated, cyclic nucleotide-modulated pacemaker channels. J Pharmacol Exp Ther 322:931–939
13. Choi KL, Mossman C, Aube J, Yellen G (1993) The internal quaternary ammonium receptor site of Shaker potassium channels. Neuron 10:533–541
14. Fernandez-Velasco M, Goren N, Benito G, Blanco-Rivero J, Bosca L, Delgado C (2003) Regional distribution of hyperpolarization-activated current (If) and hyperpolarization-activated cyclic nucleotide-gated channel mRNA expression in ventricular cells from control and hypertrophied rat hearts. J Physiol 553:395–405

15. Gauss R, Seifert R, Kaupp UB (1998) Molecular identification of a hyperpolarization-activated channel in sea urchin sperm. Nature 393:583–587
16. Henrikson CA, Xue T, Dong P, Sang D, Marban E, Li RA (2003) Identification of a surface charged residue in the S3–S4 linker of the pacemaker (HCN) channel that influences activation gating. J Biol Chem 278:13647–13654
17. Hidalgo P, MacKinnon R (1995) Revealing the architecture of a K+ channel pore through mutant cycles with a peptide inhibitor. Science 268:307–310
18. Hille B (2001) Ion channels of excitable membranes, 3rd edn. Sinauer, Sunderland
19. Lesso H, Li RA (2003) Helical secondary structure of the external S3–S4 linker of pacemaker (HCN) channels revealed by site-dependent perturbations of activation phenotype. J Biol Chem 278:22290–22297
20. Li RA, Ennis IL, French RJ, Dudley SC Jr, Tomaselli GF, Marban E (2001) Clockwise domain arrangement of the sodium channel revealed by (mu)-conotoxin (GIIIA) docking orientation. J Biol Chem 276:11072–11077
21. Li RA, Moore J, Tarasova Y, Boheler K (2005) Human embryonic stem cell-derived cardiomyocytes: therapeutic potentials and limitations. J Stem Cells 1:109–124
22. Lieu DK, Chan YC, Lau CP, Tse HF, Siu CW, Li RA (2008) Overexpression of HCN-encoded pacemaker current silences bioartificial pacemakers. Heart Rhythm 5:1310–1317
23. Ludwig A, Zong X, Jeglitsch M, Hofmann F, Biel M (1998) A family of hyperpolarization-activated mammalian cation channels. Nature 393:587–591
24. Milanesi R, Baruscotti M, Gnecchi-Ruscone T, DiFrancesco D (2006) Familial sinus bradycardia associated with a mutation in the cardiac pacemaker channel. N Engl J Med 354:151–157
25. Moosmang S, Stieber J, Zong X, Biel M, Hofmann F, Ludwig A (2001) Cellular expression and functional characterization of four hyperpolarization-activated pacemaker channels in cardiac and neuronal tissues. Eur J Biochem 268:1646–1652
26. Santoro B, Chen S, Luthi A, Pavlidis P, Shumyatsky GP, Tibbs GR, Siegelbaum SA (2000) Molecular and functional heterogeneity of hyperpolarization-activated pacemaker channels in the mouse CNS. J Neurosci 20:5264–5275
27. Santoro B, Liu DT, Yao H, Bartsch D, Kandel ER, Siegelbaum SA, Tibbs GR (1998) Identification of a gene encoding a hyperpolarization-activated pacemaker channel of brain. Cell 93:717–729
28. Santoro B, Tibbs GR (1999) The HCN gene family: molecular basis of the hyperpolarization-activated pacemaker channels. Ann N Y Acad Sci 868:741–764
29. Schulze-Bahr E, Neu A, Friederich P, Kaupp UB, Breithardt G, Pongs O, Isbrandt D (2003) Pacemaker channel dysfunction in a patient with sinus node disease. J Clin Invest 111:1537–1545
30. Shin KS, Rothberg BS, Yellen G (2001) Blocker state dependence and trapping in hyperpolarization-activated cation channels: evidence for an intracellular activation gate. J Gen Physiol 117:91–101
31. Siu CW, Lieu DK, Li RA (2006) HCN-encoded pacemaker channels: from physiology and biophysics to bioengineering. J Membr Biol 214:115–122
32. Siu CW, Moore JC, Li RA (2007) Human embryonic stem cell-derived cardiomyocytes for heart therapies. Cardiovasc Hematol Disord Drug Targets 7:145–152
33. Tsang SY, Lesso H, Li RA (2004) Critical intra-linker interactions of HCN1-encoded pacemaker channels revealed by interchange of S3–S4 determinants. Biochem Biophys Res Commun 322:652–658
34. Tsang SY, Lesso H, Li RA (2004) Dissecting the structural and functional roles of the S3–S4 linker of pacemaker (hyperpolarization-activated cyclic nucleotide-modulated) channels by systematic length alterations. J Biol Chem 279:43752–43759
35. Tse HF, Xue T, Lau CP, Siu CW, Wang K, Zhang QY, Tomaselli GF, Akar FG, Li RA (2006) Bioartificial sinus node constructed via in vivo gene transfer of an engineered pacemaker HCN channel reduces the dependence on electronic pacemaker in a sick-sinus syndrome model. Circulation 114:1000–1011
36. Ulens C, Tytgat J (2001) Functional heteromerization of HCN1 and HCN2 pacemaker channels. J Biol Chem 276:6069–6072
37. Xue T, Li RA (2002) An external determinant in the S5-P linker of the pacemaker (HCN) channel identified by sulfhydryl modification. J Biol Chem 277:46233–46242
38. Xue T, Marban E, Li RA (2002) Dominant-negative suppression of HCN1- and HCN2-encoded pacemaker currents by an engineered HCN1 construct: insights into structure-function relationships and multimerization. Circ Res 90:1267–1273
39. Xue T, Siu CW, Lieu DK, Lau CP, Tse HF, Li RA (2007) Mechanistic role of I(f) revealed by induction of ventricular automaticity by somatic gene transfer of gating-engineered pacemaker (HCN) channels. Circulation 115:1839–1850
40. Kirsch GE, Trepakova ES, Brimecombe JC, Sidach SS, Erickson HD, Kochan MC, Shyjka LM, Lacerda AE, Brown AM (2004) Variability in the measurement of hERG potassium channel inhibition: effects of temperature and stimulus pattern. J Pharmacol Toxicol Methods 50(2):93–101
41. Kasama M, Furukawa Y, Oguchi T, Hoyano Y, Chiba S (1998) Effects of low temperature on the chronotropic and inotropic responses to zatebradine, E-4031 and verapamil in isolated perfused dog atria. Jpn J Pharmacol 78(4):493–499